coupling to unwanted antitrapped states a Raman transition to the $F = 2, m = 0$ ground state of Na could be used.

An important property of the condensate, and any output-coupled fraction, is its coherence. Coherence effects between two condensates have already been observed by dropping them and allowing them to interfere (*30*). Because we use a stimulated Raman process, our output beam should be fully coherent. The effect of the mean field on the atoms as they leave the BEC will be to distort the outgoing wave without resulting in any true loss of coherence. In a separate experiment we observed matter-wave interference due to the 100-kHz phase evolution discussed above and we are using it to measure the coherence properties of the condensate.

References and Notes

1. A. Einstein, *Sitzungsbe. Kgl. Preuss. Akad. Wiss.* (1924), p. 261; *ibid.* (1925), p. 3.
2. M. H. Anderson, J. R. Ensher, M. R. Matthews, C. E. Wieman, E. A. Cornell, *Science* **269**, 198 (1995).
3. K. B. Davis *et al., Phys. Rev. Lett.* **75**, 3969 (1995).
4. C. C. Bradley, C. A. Sackett, R. G. Hulet, *ibid.* **78**, 985 (1997); see also C. C. Bradley, C. A. Sackett, J. J. Tollett, R. G. Hulet, *ibid.* **75**, 1687 (1995).
5. D. G. Fried *et al., ibid.* **81**, 3807 (1998).
6. *J. Physique* **4**, 11 (1994); *Appl. Phys. B.* **54**, 321 (1992); *J. Phys. Rep*. 240 (1994) (special issues on optics and interferometry with atoms).
7. M.-O. Mewes *et al., Phys. Rev. Lett.* **78**, 582 (1997).
8. A truly cw atom laser produces a continuous, coherent matter wave output while being continuously replenished with new atoms, in direct analogy with a cw optical laser. The coherence length of such a laser would be longer than the size of the trapped condensate just as the coherence length of a cw optical laser is longer than the laser cavity.
9. G. Moy, J. Hope, C. Savage, *Phys. Rev. A* **55**, 3631 (1997).
10. M. A. Edwards, C. W. Clark, K. Burnett, S. L. Rolston, W. D. Phillips, *J. Phys. B*, in press.
11. M. Kozuma *et al., Phys. Rev. Lett.* **82**, 871 (1999).
12. Our TOP trap is different from previous TOP traps (*13*) because the rotating bias field orbits in a plane that includes the quadrupole axis. The field gradient along the quadrupole axis ($\hat{z}$) is 9.2 T/m, and the rotating bias field is 1.0 mT. The time-averaged magnetic field forms a trap with harmonic frequencies $\omega_x/2\pi = 180$ Hz, $\omega_y/2\pi = 250$ Hz, and $\omega_z/2\pi = 360$ Hz.
13. W. Petrich, M. H. Anderson, J. R. Ensher, E. A. Cornell, *Phys. Rev. Lett.* **74**, 3352 (1995).
14. Atoms in the state $m = -1$ are trapped by the magnetic fields, whereas those in state $m = +1$ are antitrapped. The state $m = 0$ does not feel the confining potential of the magnetic trap.
15. This was done by switching off the trap and measuring the rate of the mean-field-driven ballistic expansion of the condensate at long times (>10 ms).
16. All uncertainties reported in this paper are 1-SD combined statistical and systematic uncertainties.
17. For frequency stability, both beams are derived from a single dye laser with the frequency difference controlled by two acousto-optical modulators.
18. θ, which equals 166° in this case, is the angle between $\boldsymbol{k}_1$ and $\boldsymbol{k}_2$, and $|\boldsymbol{k}_1| \approx |\boldsymbol{k}_2| = k$. Therefore, $P = 1.99\hbar k \approx 2\hbar k$.
19. We define $\Delta m = m_{final} - m_{initial}$. $m_{initial} = -1$ is the only magnetically trapped state.
20. Assuming that the scattering lengths among all m states are the same, this can be derived from expressions found in [F. Dalfovo, S. Giorgini, L. P. Pitaevskii, S. Stringari, *Rev. Mod. Phys.* **71**, 2 (1999)]. The energy needed to add one atom is μ, which has a magnetic contribution of 3/7 μ and a mean-field contribution of 4/7 μ. If a small number of atoms are ouput-coupled to $m = 0$, a state that is not magnetically trapped, their release energy will simply be 4/7 μ, or twice the average release energy of 2/7 μ for the whole condensate.
21. In addition, the longitudinal momentum width is reduced by about the same factor because of kinematic compression.
22. The characteristic time during which the mean field potential energy turns into kinetic energy in the released BEC is $1/\bar{\omega}$ (in our case about 6 ms), where $\bar{\omega}$ is the geometric mean of the three trapping frequencies. For our two-photon Raman transition the characteristic time scale for leaving the region of the condensate is 300 μs.
23. This is because our TOP field rotates in $\hat{x}$-$\hat{z}$ plane, which includes the direction of gravity.
24. The power quoted was the average over a 3-mm-diameter aperture in the center of a somewhat inhomogeneous 7-mm beam. These powers were empirically chosen to produce good output coupling.
25. The resonance frequency, for the $\Delta m = 2$ four-photon transition discussed later, was found to be 6.15(5) MHz, in good agreement with the calculated value of 6.0(2) MHz based on measurements of the trapping magnetic fields. This additional detuning of 2×250 kHz = 500 kHz from the four-photon resonance frequency is large compared with the Fourier width of the Raman pulse and results in a suppression of coupling to the $4\hbar k\hat{z}$, $m = +1$ state.
26. A stimulated Raman transition that changes the momentum state of an atom but does not change the internal energy state can be viewed as Bragg diffraction (*11*); see also P. J. Martin, B. G. Oldaker, A. H. Miklich, D. E. Pritchard, *Phys. Rev. Lett.* **60**, 515 (1988).
27. Because of our choice of applying the Raman beams along the quadrupole axis of the trap ($\hat{z}$), the trajectory of the output-coupled atoms (initially along $\hat{z}$) lies in the $\hat{x}$-$\hat{z}$ plane because gravity is along $\hat{x}$. This is the plane of the rotating magnetic field zero and so the atoms will, at some point in time, cross this circle of death.
28. In the case of $\theta = 180°$ the recoil momentum from a first-order Raman transition is exactly $2\hbar k\hat{z}$, which corresponds to a frequency of 100.1 kHz.
29. This was confirmed in a separate experiment, which looked at the interference of two clouds of atoms diffracted out of the condensate.
30. If the output coupling process were made continuous, by using an optical dipole or magnetic trap with no time-dependent magnetic fields, such coupling would not occur because the Fourier width of the light pulse could be made arbitrarily small. It would therefore be a simple matter to make a continuous Raman output coupler in such a case.
31. M. R. Andrews *et al., Science* **273**, 637 (1997).

32. Supported in part by the Office of Naval Research and NASA. M.K. acknowledges the support of the Japanese Society for the Promotion of Science for Young Scientists. We thank C. W. Clark, M. A. Edwards, and P. S. Julienne for their valuable comments and suggestions.

24 November 1998; accepted 3 February 1999

Quantum-Well States as Fabry-Pérot Modes in a Thin-Film Electron Interferometer

J. J. Paggel, T. Miller, T.-C. Chiang*

Angle-resolved photoemission from atomically uniform silver films on iron (100) shows quantum-well states for absolutely determined film thicknesses ranging from 1 to ~100 monolayers. These states can be understood in terms of Fabry-Pérot modes in an electron interferometer. A quantitative line shape analysis over the entire two orders of magnitude of thickness range yields an accurate measurement of the band structure, quasiparticle lifetime, electron reflectivity, and phase shift. Effects of confinement energy gap, reflection loss, and surface scattering caused by controlled roughness are demonstrated.

Quantum mechanics is based on wave-particle duality, which is well documented through diffraction and interference experiments using particles (*1*). Thus, there is a close analogy between a standing electromagnetic wave between two reflecting surfaces and an electron confined in a square potential well (*2*). The former case corresponds to the Fabry-Pérot interferometer (*3*), which shows a set of peaks in optical transmission. The latter case, an electron quantum well, can be realized in a thin solid film. Electron confinement within a film results in discrete quantum-well states observable by angle-resolved photoemission (*4*). Photoemission, however, involves an optical transition. This can lead to complications, and the line shape is generally quite complex even for simple systems (*5, 6*). Nevertheless, we show here that photoemission spectra of quantum-well states can be analyzed in the same way as an optical Fabry-Pérot interferometer filled with a medium. The dispersive and absorptive properties of this medium account for the electronic band structure and quasiparticle lifetime.

The Ag on Fe(100) system was chosen for this study because of its rather unique property that atomically uniform films can be prepared for thicknesses ranging from 1 to ~100 monolayers (ML) (*7*). Layer counting leads to an absolute determination of thickness, and a sin-

Department of Physics, University of Illinois, 1110 West Green Street, Urbana, IL 61801, USA, and Frederick Seitz Materials Research Laboratory, University of Illinois, 104 South Goodwin Avenue, Urbana, IL 61801, USA.

*To whom correspondence should be addressed. E-mail: t-chiang@uiuc.edu

gle Fabry-Pérot formula describes the results over the entire two orders of magnitude of thickness range. The large redundancy of the data set yields accurate measurements of the band structure, quasiparticle lifetime, electron reflectivity, and phase shift. These quantities are of basic importance to solid state physics and interface science, and yet only fragmentary and qualitative information was available previously. The capabilities of quantum-well spectroscopy, though recognized long ago (*8*), are fully realized because of atomic-level control of film growth. Effects of surface scattering caused by film roughness are investigated by cold condensation of Ag onto an otherwise atomically uniform film, and the results illustrate the connection between interferometer finesse and quasiparticle lifetime.

Angle-resolved photoemission spectra (Fig. 1) were taken with a normal-emission geometry for Ag films of various coverages at a temperature of 100 K. The peaks are quantum-well states derived from the Ag *sp* valence electrons. All of these films are atomically uniform, except for the 27.5-ML and 42.5-ML coverages. The 27.5-ML spectrum consists of two sets of peaks, one corresponding to a thickness of 27 ML and the other 28 ML, suggesting that the film is a mixture of the two discrete thicknesses. Likewise, the 42.5-ML spectrum consists of two sets of peaks corresponding to 42 and 43 ML. In each of the other cases, the coverage is an integer number of monolayers, and the spectrum shows just one set of peaks.

These films were prepared by depositing Ag onto a Fe(100) whisker kept at 100 K followed by annealing to 300°C (*7*). Additional Ag can be added by deposition at low temperatures followed by annealing in the same manner. Repeating this procedure with small increments of Ag allows one to follow the evolution of the film from one integer monolayer thickness to the next. Sufficient data have been taken to establish the absolute quantum-well peak positions in the thickness range of 1 to 20 ML on a monolayer-by-monolayer basis. The resulting data set is large enough to carry out a full analysis to establish a unique correspondence between film thickness and quantum-well peak positions for any thickness. The thicknesses cited in Fig. 1 are determined in this way and can be regarded as absolute.

The qualitative features of the spectra are easily understood. The nearly free-electron–like Ag *sp* electrons are confined in the film, resulting in quantum-well peaks. Traditional discussion begins with the Bohr-Sommerfeld quantization rule,

$$2k(E)Nt + \Phi(E) = 2n\pi \qquad (1)$$

(*9, 10*), where $k(E)$ is the electron wave vector as a function of binding energy, N is the film thickness in monolayers, t = 2.04 Å is the monolayer thickness, Φ is the total boundary phase shift (sum of the phase shifts at the surface and the interface), and n is the quantum number. Although this formula is useful for peak position analysis, it does not explain the line shape or linewidth.

A deeper understanding of the photoemission process must involve wave functions. The final state is a time-reversed low-energy electron diffraction (TRLEED) state (*11*). The initial state corresponds to an electron traveling from inside of the crystal toward the crystal surface, which is photoexcited into the TRLEED state and enters the detector to complete the electrical circuit. In the case of a quantum well, the initial state undergoes multiple reflections between the two boundaries, and becomes modulated by an interference factor

$$\frac{1}{1 - R\exp[i(2kNt + \Phi)]\exp(-Nt/\lambda)} \qquad (2)$$

where R is the product of the reflectivities at the surface and the interface, and λ is the quasiparticle mean free path. The mean free path gives rise to damping, and is related to the quasiparticle inverse lifetime Γ via the group velocity v by $\Gamma = v/\lambda$.

Under our experimental conditions, the spectrum for bulk single-crystal Ag is a smooth, featureless continuum dominated by surface

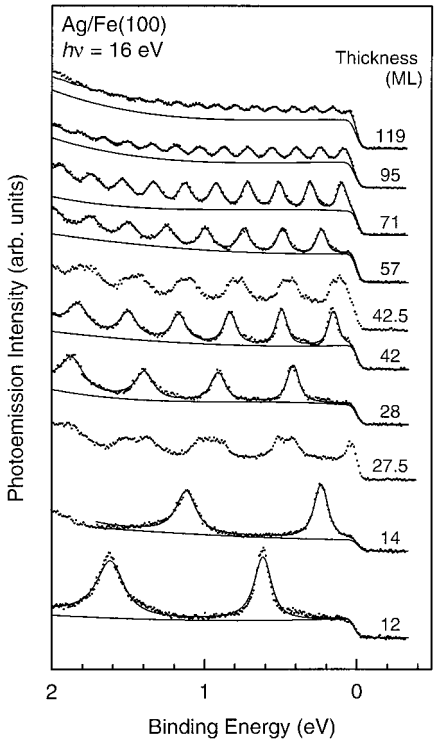

Fig. 1. Normal emission spectra (dots) for Ag on Fe(100) at various coverages. Also shown are the fits and background functions (curves).

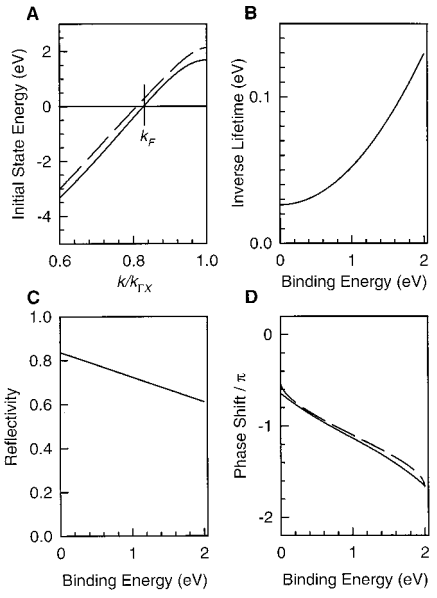

Fig. 2. (**A**) Dispersion relation for the Ag *sp* band (solid curve) and the result of a band structure calculation by Eckardt *et al.* (*15*) (dashed curve). The Fermi wave vector k_F is marked. (**B**) Quasiparticle inverse lifetime. (**C**) Reflectivity. (**D**) Phase shift in units of π (solid curve) and the result from a semiempirical formula (dashed curve).

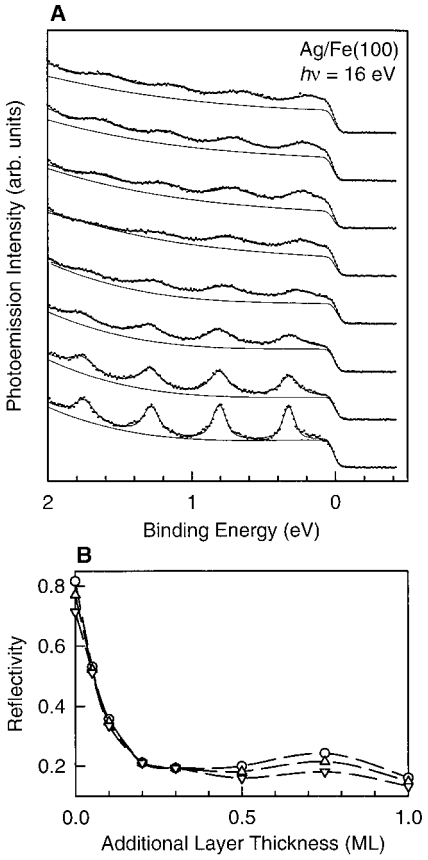

Fig. 3. (**A**) Normal emission spectra (dots), fits (curves), and background functions (curves) for Ag film thicknesses of 29, 29.05, 29.1, 29.2, 29.3, 29.5, 29.75, and 30 ML (from bottom to top). (**B**) Reflectivity at a binding energy of 0 eV (○), 0.8 eV (△), and 1.80 eV (▽) as a function of added Ag thickness.

photoemission (*5*). In the case of a quantum well, the optical transition matrix element, relative to the bulk case, is modulated by the interference factor given in Eq. 2. The photoemission intensity, in turn, is modulated by the absolute square of the same factor. Thus, the spectrum for a quantum well becomes

$$I \propto \frac{1}{1 + \left(\frac{4f^2}{\pi^2}\right)\sin^2\left(kNt + \frac{\Phi}{2}\right)} A(E) + B(E) \quad (3)$$

where A is a smooth function of E, its prefactor comes from the absolute square of the interference factor, and B is a smooth background function due to inelastic scattering and incoherent emission. The quantity f is the Fabry-Pérot finesse (*3*) (ratio of peak separation to peak width) given by

$$f = \frac{\pi(R)^{1/2}\exp(-Nt/2\lambda)}{1 - R\exp(-Nt/\lambda)} \quad (4)$$

Equations 3 and 4 are the same as the usual Fabry-Pérot formula for an interferometer filled with an absorptive medium.

Equation 3 yields a set of peaks at positions where the sine function in the denominator equals zero; the resulting condition is just the Bohr-Sommerfeld quantization rule given in Eq. 1. The peak width δE depends on N, R, and λ:

$$\delta E = \Gamma\eta \frac{1 - R\exp(-1/\eta)}{R^{1/2}\exp[-1/(2\eta)]} \quad (5)$$

where $\eta = \lambda/(Nt)$. Generally, δE is greater than Γ, except when $R = 1$ (ideal quantum well) and $\lambda \gg Nt$ (large mean free path). In that case, the measured width equals the quasiparticle inverse lifetime. As will be seen below, $R < 1$ for our quantum wells. The peaks in Fig. 1 are thus broadened. This broadening is relatively minor for the thicker films, but can be quite noticeable for thinner films (because of loss caused by more frequent reflections). The peaks become narrower near the Fermi level, mostly because of a smaller Γ at lower binding energy.

The quantities k and Γ (related to the real and imaginary parts of the band dispersion relations) and R and Φ (related to the confinement potentials) are of basic interest and completely specify the interferometer properties. Whereas k and Φ are related to the peak positions through Eq. 1, Γ and R are related to the peak width through Eq. 5. They all depend on E, but not on N. Thus, a set of data spanning a wide range in N allows a unique determination (and cross-checks) of these four quantities at a given E. We have adopted a fitting procedure to deduce these quantities. The band structure $k(E)$ is parameterized using a two-band model (*9*), and the other three quantities are modeled by quadratic functions of E. In addition, A in Eq. 3 is taken to be a polynomial of E (up to fourth order and no higher than the number of peaks in each spectrum), and B is also a polynomial (fourth order for the 119-ML spectrum, and third order for the rest). The resulting values of k, Γ, Φ, and R (Fig. 2) and the corresponding fits to the data (solid curves in Fig. 1) are shown. The fits are excellent for all thicknesses except for $N = 1$ and 2, where the peak positions deviate from the model by up to ~100 meV. At such small film thicknesses, the two boundaries of the film overlap and can no longer be modeled accurately by separate, independent phase shifts.

Our experimental band dispersion (solid curve in Fig. 2A) crosses the Fermi level at the Fermi wave vector $k_F/k_{\Gamma X} = 0.828 \pm 0.002$, which is very close to the value of 0.819 ± 0.002 obtained from de Haas–van Alphen data taken at ~1 K (*12*). The discrepancy may be partly attributable to the temperature difference (*13*). Our value for the Fermi velocity in the [100] direction is 1.065 ± 0.010 in units of the free-electron Fermi velocity, whereas the de Haas–van Alphen value deduced from a temperature-dependent amplitude measurement is 0.97 ± 0.03 (*14*). Also shown in Fig. 2A for comparison is a representative band structure calculation by Eckardt *et al.* based on a relativistic self-consistent method (*15*). The difference is much larger than our statistical uncertainty of 0.03 eV.

The quasiparticle inverse lifetime (Fig. 2B) exhibits an E^2 dependence; the linear term included in the fit becomes negligibly small. This E^2 dependence is consistent with theoretical predictions based on a dominant Auger contribution to the quasiparticle decay (*16*). The residual width at the Fermi level, 25 meV, is not zero, even though the Auger decay rate vanishes. Part of this is due to phonon scattering, and a temperature-dependent measurement yields a phonon contribution of ~14 meV at 100 K by extrapolation. The remaining 11 meV can be attributed to scattering by defects and trace impurities. This represents the narrowest quasiparticle linewidth ever determined by photoemission from a bulk state.

The reflectivity (Fig. 2C) is close to but less than unity, suggesting that the interface potential at the Ag-Fe interface is not fully confining. This is not surprising, because a hybridization gap (rather than an absolute gap) provides the confinement potential (*10*). Another factor is that the lattice mismatch between Ag and Fe, though small, could lead to nonspecular reflection, resulting in a reduced specular reflectivity.

The phase shift (solid curve in Fig. 2D) decreases by ~π over the energy range of interest. This is expected, because the phase shift at the Ag-Fe interface should decrease by π across the hybridization gap in Fe. The phase variation, but not the absolute phase shift itself, can be estimated using a semiempirical formula (*10*). This estimate, with an arbitrary vertical offset, is shown as the dashed curve (*17*) and is in good agreement with our result.

A set of spectra starting from an atomically uniform 29-ML film with additional amounts of Ag deposited on the surface at 100 K without annealing is shown in Fig. 3A. The cold condensation roughens the surface by a frosting effect. As a result, the specular reflectivity decreases, the interferometer finesse decreases correspondingly, and the quantum-well peaks broaden. The effect is large even for depositions as small as 0.05 ML, illustrating the extreme sensitivity of the peak width to imperfections. The same Fabry-Pérot formula yields the fits shown in Fig. 3A. The reflectivity R, deduced from the fit at various binding energies and shown in Fig. 3B as a function of the additional Ag deposit, decays rapidly and exhibits a weak maximum near 1 ML additional coverage. This is somewhat similar to the damped oscillations as observed by reflection high-energy electron diffraction during rough film growth. The peak width broadening (Fig. 3A) is equivalent to a reduction in quasiparticle lifetime as a result of surface scattering.

References and Notes

1. G. Badurek, H. Rauch, A. Zeilinger, Eds., *Proceedings of the International Workshop on Matter Wave Interferometry,* Vienna (North-Holland, Amsterdam, 1988), published in *Physica B* **151**, 1–400 (1988); C. Jörnsson, *Z. Phys.* **161**, 454 (1961).
2. C. Cohen-Tannoudji, B. Diu, F. Laloë, *Quantum Mechanics* (Wiley, New York, 1977).
3. M. Born and E. Wolf, *Principles of Optics* (Pergamon, New York, ed. 6, 1980).
4. S. Å. Lindgren and L. Waldén, *Phys. Rev. Lett.* **61**, 2894 (1988); T. Miller, A. Samsavar, G. E. Franklin, T.-C. Chiang, *ibid.*, p. 1404.
5. T. Miller, W. E. McMahon, T.-C. Chiang, *ibid.* **77**, 1167 (1996).
6. E. D. Hansen, T. Miller, T.-C. Chiang, *ibid.* **80**, 1766 (1998).
7. J. J. Paggel, T. Miller, T.-C. Chiang, *ibid.* **81**, 5632 (1998).
8. P. D. Loly and J. B. Pendry, *J. Phys. C* **16**, 423 (1983).
9. M. A. Mueller, T. Miller, T.-C. Chiang, *Phys. Rev. B* **41**, 5214 (1990).
10. N. V. Smith, N. B. Brookes, Y. Chang, P. D. Johnson, *ibid.* **49**, 332 (1994).
11. S. Hüfner, *Photoelectron Spectroscopy* (Springer-Verlag, Berlin, ed. 2, 1996).
12. P. T. Coleridge and I. M. Templeton, *Phys. Rev. B* **25**, 7818 (1982).
13. Some experiments suggest that the error of the de Haas–van Alphen measurement might be larger than expected. See C. A. Steele and R. G. Goodrich, *Phys. Rev. B* **24**, 6129 (1981).
14. M. R. Halse, *Philos. Trans. R. Soc. London* **265**, 507 (1969).
15. H. Eckardt, L. Fritsche, J. Noffke, *J. Phys. F* **14**, 97 (1984).
16. D. Pines and P. Nozières, *The Theory of Quantum Liquids* (Benjamin, New York, 1966).
17. The E_l and E_u parameters (binding energies of the lower and upper edges of the hybridization gap, respectively) in (*10*) are not known precisely. They are chosen to be 2.0 and 0.0 eV, respectively.

18. Supported by NSF grants DMR-95-31582 and DMR-95-31809. We thank the Petroleum Research Fund and the U.S. Department of Energy, Division of Materials Sciences (grant DEFG02-91ER45439) for partial support of the synchrotron beamline operation and the central facilities of the Materials Research Laboratory. The Synchrotron Radiation Center, where the experiment was carried out, is supported by NSF grant DMR-95-31009.

30 November 1998; accepted 8 February 1999

Quantum-Well States as Fabry-Pérot Modes in a Thin-Film Electron Interferometer

J. J. Paggel *et al.*

Science **283**, 1709 (1999);
DOI: 10.1126/science.283.5408.1709

Science (print ISSN 0036-8075; online ISSN 1095-9203) is published weekly, except the last week in December, by the American Association for the Advancement of Science, 1200 New York Avenue NW, Washington, DC 20005.